ΔϕΔη correlations in central Au+Au collisions at √sNN=200 GeV

(STAR Collaboration) Adams, J.; ...; Planinić, Mirko; ...; Poljak, Nikola; ...; Zuo, J. X.

Source / Izvornik: **Physical Review C - Nuclear Physics, 2007, 75**

Journal article, Published version
Rad u časopisu, Objavljena verzija rada (izdavačev PDF)

https://doi.org/10.1103/PhysRevC.75.034901

Permanent link / Trajna poveznica: https://urn.nsk.hr/urn:nbn:hr:217:446288

$\Delta\phi\Delta\eta$ correlations in central Au+Au collisions at $\sqrt{s_{NN}} = 200$ GeV

J. Adams,[2] M. M. Aggarwal,[29] Z. Ahammed,[44] J. Amonett,[19] B. D. Anderson,[19] M. Anderson,[6] D. Arkhipkin,[12] G. S. Averichev,[11] Y. Bai,[27] J. Balewski,[16] O. Barannikova,[32] L. S. Barnby,[2] J. Baudot,[17] S. Bekele,[28] V. V. Belaga,[11] A. Bellingeri-Laurikainen,[39] R. Bellwied,[47] B. I. Bezverkhny,[49] S. Bharadwaj,[34] A. Bhasin,[18] A. K. Bhati,[29] H. Bichsel,[46] J. Bielcik,[49] J. Bielcikova,[49] L. C. Bland,[3] C. O. Blyth,[2] S.-L. Blyth,[21] B. E. Bonner,[35] M. Botje,[27] J. Bouchet,[39] A. V. Brandin,[25] A. Bravar,[3] M. Bystersky,[10] R. V. Cadman,[1] X. Z. Cai,[38] H. Caines,[49] M. Calderón de la Barca Sánchez,[6] J. Castillo,[27] O. Catu,[49] D. Cebra,[6] Z. Chajecki,[28] P. Chaloupka,[10] S. Chattopadhyay,[44] H. F. Chen,[37] J. H. Chen,[38] Y. Chen,[7] J. Cheng,[42] M. Cherney,[9] A. Chikanian,[49] H. A. Choi,[33] W. Christie,[3] J. P. Coffin,[17] T. M. Cormier,[47] M. R. Cosentino,[36] J. G. Cramer,[46] H. J. Crawford,[5] D. Das,[44] S. Das,[44] M. Daugherity,[41] M. M. de Moura,[36] T. G. Dedovich,[11] M. DePhillips,[3] A. A. Derevschikov,[31] L. Didenko,[3] T. Dietel,[13] P. Djawotho,[16] S. M. Dogra,[18] W. J. Dong,[7] X. Dong,[37] J. E. Draper,[6] F. Du,[49] V. B. Dunin,[11] J. C. Dunlop,[3] M. R. Dutta Mazumdar,[44] V. Eckardt,[23] W. R. Edwards,[21] L. G. Efimov,[11] V. Emelianov,[25] J. Engelage,[5] G. Eppley,[35] B. Erazmus,[39] M. Estienne,[17] P. Fachini,[3] R. Fatemi,[22] J. Fedorisin,[11] K. Filimonov,[21] P. Filip,[12] E. Finch,[49] V. Fine,[3] Y. Fisyak,[3] J. Fu,[48] C. A. Gagliardi,[40] L. Gaillard,[2] J. Gans,[49] M. S. Ganti,[44] V. Ghazikhanian,[7] P. Ghosh,[44] J. E. Gonzalez,[7] Y. G. Gorbunov,[9] H. Gos,[45] O. Grebenyuk,[27] D. Grosnick,[43] S. M. Guertin,[7] K. S. F. F. Guimaraes,[36] Y. Guo,[47] N. Gupta,[18] T. D. Gutierrez,[6] B. Haag,[6] T. J. Hallman,[3] A. Hamed,[47] J. W. Harris,[49] W. He,[16] M. Heinz,[49] T. W. Henry,[40] S. Hepplemann,[30] B. Hippolyte,[17] A. Hirsch,[32] E. Hjort,[21] G. W. Hoffmann,[41] M. J. Horner,[21] H. Z. Huang,[7] S. L. Huang,[37] E. W. Hughes,[4] T. J. Humanic,[28] G. Igo,[7] P. Jacobs,[21] W. W. Jacobs,[16] P. Jakl,[10] F. Jia,[20] H. Jiang,[7] P. G. Jones,[2] E. G. Judd,[5] S. Kabana,[39] K. Kang,[42] J. Kapitan,[10] M. Kaplan,[8] D. Keane,[19] A. Kechechyan,[11] V. Yu. Khodyrev,[31] B. C. Kim,[33] J. Kiryluk,[22] A. Kisiel,[45] E. M. Kislov,[11] S. R. Klein,[21] D. D. Koetke,[43] T. Kollegger,[13] M. Kopytine,[19] L. Kotchenda,[25] V. Kouchpil,[10] K. L. Kowalik,[21] M. Kramer,[26] P. Kravtsov,[25] V. I. Kravtsov,[31] K. Krueger,[1] C. Kuhn,[17] A. I. Kulikov,[11] A. Kumar,[29] A. A. Kuznetsov,[11] M. A. C. Lamont,[49] J. M. Landgraf,[3] S. Lange,[13] S. LaPointe,[47] F. Laue,[3] J. Lauret,[3] A. Lebedev,[3] R. Lednicky,[12] C.-H. Lee,[33] S. Lehocka,[11] M. J. LeVine,[3] C. Li,[37] Q. Li,[47] Y. Li,[42] G. Lin,[49] S. J. Lindenbaum,[26] M. A. Lisa,[28] F. Liu,[48] H. Liu,[37] J. Liu,[35] L. Liu,[48] Z. Liu,[48] T. Ljubicic,[3] W. J. Llope,[35] H. Long,[7] R. S. Longacre,[3] M. Lopez-Noriega,[28] W. A. Love,[3] Y. Lu,[48] T. Ludlam,[3] D. Lynn,[3] G. L. Ma,[38] J. G. Ma,[7] Y. G. Ma,[38] D. Magestro,[28] D. P. Mahapatra,[14] R. Majka,[49] L. K. Mangotra,[18] R. Manweiler,[43] S. Margetis,[19] C. Markert,[19] L. Martin,[39] H. S. Matis,[21] Yu. A. Matulenko,[31] C. J. McClain,[1] T. S. McShane,[9] Yu. Melnick,[31] A. Meschanin,[31] M. L. Miller,[22] N. G. Minaev,[31] S. Mioduszewski,[40] C. Mironov,[19] A. Mischke,[27] D. K. Mishra,[14] J. Mitchell,[35] B. Mohanty,[44] L. Molnar,[32] C. F. Moore,[41] D. A. Morozov,[31] M. G. Munhoz,[36] B. K. Nandi,[15] C. Nattrass,[49] T. K. Nayak,[44] J. M. Nelson,[2] P. K. Netrakanti,[44] V. A. Nikitin,[12] L. V. Nogach,[31] S. B. Nurushev,[31] G. Odyniec,[21] A. Ogawa,[3] V. Okorokov,[25] M. Oldenburg,[21] D. Olson,[21] M. Pachr,[10] S. K. Pal,[44] Y. Panebratsev,[11] S. Y. Panitkin,[3] A. I. Pavlinov,[47] T. Pawlak,[45] T. Peitzmann,[27] V. Perevoztchikov,[3] C. Perkins,[5] W. Peryt,[45] V. A. Petrov,[47] S. C. Phatak,[14] R. Picha,[6] M. Planinic,[50] J. Pluta,[45] N. Poljak,[50] N. Porile,[32] J. Porter,[46] A. M. Poskanzer,[21] M. Potekhin,[3] E. Potrebenikova,[11] B. V. K. S. Potukuchi,[18] D. Prindle,[46] C. Pruneau,[47] J. Putschke,[21] G. Rakness,[30] R. Raniwala,[34] S. Raniwala,[34] R. L. Ray,[41] S. V. Razin,[11] J. Reinnarth,[39] D. Relyea,[4] F. Retiere,[21] A. Ridiger,[25] H. G. Ritter,[21] J. B. Roberts,[35] O. V. Rogachevskiy,[11] J. L. Romero,[6] A. Rose,[21] C. Roy,[39] L. Ruan,[21] M. J. Russcher,[27] R. Sahoo,[14] I. Sakrejda,[21] S. Salur,[49] J. Sandweiss,[49] M. Sarsour,[40] P. S. Sazhin,[11] J. Schambach,[41] R. P. Scharenberg,[32] N. Schmitz,[23] K. Schweda,[21] J. Seger,[9] I. Selyuzhenkov,[47] P. Seyboth,[23] A. Shabetai,[21] E. Shahaliev,[11] M. Shao,[37] M. Sharma,[29] W. Q. Shen,[38] S. S. Shimanskiy,[11] E. Sichtermann,[21] F. Simon,[22] R. N. Singaraju,[44] N. Smirnov,[49] R. Snellings,[27] G. Sood,[43] P. Sorensen,[3] J. Sowinski,[16] J. Speltz,[17] H. M. Spinka,[1] B. Srivastava,[32] A. Stadnik,[11] T. D. S. Stanislaus,[43] R. Stock,[13] A. Stolpovsky,[47] M. Strikhanov,[25] B. Stringfellow,[32] A. A. P. Suaide,[36] E. Sugarbaker,[28] M. Sumbera,[10] Z. Sun,[20] B. Surrow,[22] M. Swanger,[9] T. J. M. Symons,[21] A. Szanto de Toledo,[36] A. Tai,[7] J. Takahashi,[36] A. H. Tang,[3] T. Tarnowsky,[32] D. Thein,[7] J. H. Thomas,[21] A. R. Timmins,[2] S. Timoshenko,[25] M. Tokarev,[11] S. Trentalange,[7] R. E. Tribble,[40] O. D. Tsai,[7] J. Ulery,[32] T. Ullrich,[3] D. G. Underwood,[1] G. Van Buren,[3] N. van der Kolk,[27] M. van Leeuwen,[21] A. M. Vander Molen,[24] R. Varma,[15] I. M. Vasilevski,[12] A. N. Vasiliev,[31] R. Vernet,[17] S. E. Vigdor,[16] Y. P. Viyogi,[44] S. Vokal,[11] S. A. Voloshin,[47] W. T. Waggoner,[9] F. Wang,[32] G. Wang,[19] J. S. Wang,[20] X. L. Wang,[37] Y. Wang,[42] J. W. Watson,[19] J. C. Webb,[16] G. D. Westfall,[24] A. Wetzler,[21] C. Whitten Jr.,[7] H. Wieman,[21] S. W. Wissink,[16] R. Witt,[49] J. Wood,[7] J. Wu,[37] N. Xu,[21] Q. H. Xu,[21] Z. Xu,[3] P. Yepes,[35] I.-K. Yoo,[33] V. I. Yurevich,[11] W. Zhan,[20] H. Zhang,[3] W. M. Zhang,[19] Y. Zhang,[37] Z. P. Zhang,[37] Y. Zhao,[37] C. Zhong,[38] R. Zoulkarneev,[12] Y. Zoulkarneeva,[12] A. N. Zubarev,[11] and J. X. Zuo[38]

(STAR Collaboration)

[1]*Argonne National Laboratory, Argonne, Illinois 60439, USA*
[2]*University of Birmingham, Birmingham, United Kingdom*
[3]*Brookhaven National Laboratory, Upton, New York 11973, USA*
[4]*California Institute of Technology, Pasadena, California 91125, USA*
[5]*University of California, Berkeley, California 94720, USA*
[6]*University of California, Davis, California 95616, USA*
[7]*University of California, Los Angeles, California 90095, USA*
[8]*Carnegie Mellon University, Pittsburgh, Pennsylvania 15213, USA*
[9]*Creighton University, Omaha, Nebraska 68178, USA*

[10]*Nuclear Physics Institute AS CR, 25068* Řež/*Prague, Czech Republic*
[11]*Laboratory for High Energy (JINR), Dubna, Russia*
[12]*Particle Physics Laboratory (JINR), Dubna, Russia*
[13]*University of Frankfurt, Frankfurt, Germany*
[14]*Institute of Physics, Bhubaneswar 751005, India*
[15]*Indian Institute of Technology, Mumbai, India*
[16]*Indiana University, Bloomington, Indiana 47408, USA*
[17]*Institut de Recherches Subatomiques, Strasbourg, France*
[18]*University of Jammu, Jammu 180001, India*
[19]*Kent State University, Kent, Ohio 44242, USA*
[20]*Institute of Modern Physics, Lanzhou, People's Republic of China*
[21]*Lawrence Berkeley National Laboratory, Berkeley, California 94720, USA*
[22]*Massachusetts Institute of Technology, Cambridge, MA 02139, USA*
[23]*Max-Planck-Institut für Physik, Munich, Germany*
[24]*Michigan State University, East Lansing, Michigan 48824, USA*
[25]*Moscow Engineering Physics Institute, Moscow, Russia*
[26]*City College of New York, New York City, New York 10031, USA*
[27]*NIKHEF and Utrecht University, Amsterdam, The Netherlands*
[28]*Ohio State University, Columbus, Ohio 43210, USA*
[29]*Panjab University, Chandigarh 160014, India*
[30]*Pennsylvania State University, University Park, Pennsylvania 16802, USA*
[31]*Institute of High Energy Physics, Protvino, Russia*
[32]*Purdue University, West Lafayette, Indiana 47907, USA*
[33]*Pusan National University, Pusan, Republic of Korea*
[34]*University of Rajasthan, Jaipur 302004, India*
[35]*Rice University, Houston, Texas 77251, USA*
[36]*Universidade de Sao Paulo, Sao Paulo, Brazil*
[37]*University of Science & Technology of China, Hefei 230026, People's Republic of China*
[38]*Shanghai Institute of Applied Physics, Shanghai 201800, People's Republic of China*
[39]*SUBATECH, Nantes, France*
[40]*Texas A&M University, College Station, Texas 77843, USA*
[41]*University of Texas, Austin, Texas 78712, USA*
[42]*Tsinghua University, Beijing 100084, People's Republic of China*
[43]*Valparaiso University, Valparaiso, Indiana 46383, USA*
[44]*Variable Energy Cyclotron Centre, Kolkata 700064, India*
[45]*Warsaw University of Technology, Warsaw, Poland*
[46]*University of Washington, Seattle, Washington 98195, USA*
[47]*Wayne State University, Detroit, Michigan 48201, USA*
[48]*Institute of Particle Physics, CCNU (HZNU), Wuhan 430079, People's Republic of China*
[49]*Yale University, New Haven, Connecticut 06520, USA*
[50]*University of Zagreb, Zagreb, HR-10002, Croatia*

(Received 6 July 2006; published 8 March 2007)

We report charged particle pair correlation analyses in the space of $\Delta\phi$ (azimuth) and $\Delta\eta$ (pseudorapidity), for central Au+Au collisions at $\sqrt{s_{NN}} = 200$ GeV in the STAR detector. The analysis involves unlike-sign charged pairs and like-sign charged pairs, which are transformed into charge-dependent (CD) signals and charge-independent (CI) signals. We present detailed parametrizations of the data. A model featuring dense gluonic hot spots as first proposed by Van Hove predicts that the observables under investigation would have sensitivity to such a substructure should it occur, and the model also motivates selection of transverse momenta in the range $0.8 < p_t < 2.0$ GeV/c. Both CD and CI correlations of high statistical significance are observed, and possible interpretations are discussed.

DOI: 10.1103/PhysRevC.75.034901 PACS number(s): 25.75.Gz, 12.38.Mh, 12.38.Qk

I. INTRODUCTION

The search for a quark-gluon plasma (QGP) [1,2] has been a high priority task at the BNL Relativistic Heavy Ion Collider (RHIC) [3]. Central Au+Au collisions at RHIC exceed [4] the initial energy density that is predicted by lattice QCD to be sufficient for production of QGP [5]. Van Hove and others [6–8] have proposed that bubbles localized in phase space (dense gluon-dominated hot spots) could be the

sources of the final state hadrons from a QGP. Such structures would have smaller spatial dimensions than the region of the fireball viewed in this midrapidity experiment, and the correlations resulting from these smaller structures might persist in the final state of the collision. The bubble hypothesis has motivated this study, and the model described in Ref. [8] has led to our selection of transverse momenta in the range $0.8 < p_t < 2.0$ GeV/c. The Hanbury-Brown and Twiss (HBT) results demonstrate that for $\sqrt{s_{NN}} = 200$ GeV, midrapidity central Au+Au, when $p_t > 0.8$ GeV/c, the average final state space geometry for pairs close in momentum is approximately describable by dimensions of around 2 fm [9]. This should lead to observable modification to the $\Delta\eta\Delta\phi$ correlation. The present experimental analysis is model independent, and it probes correlations that could have a range of explanations.

We present an analysis of charged particle pair correlations in two dimensions—$\Delta\phi$ and $\Delta\eta$—based on 2 million central Au+Au events observed in the STAR detector at $\sqrt{s_{NN}} =$ 200 GeV [10].[1] The analysis leads to a multiterm correlation function (Secs. III C and III E) which fits the $\Delta\eta$-$\Delta\phi$ distribution well. It includes terms describing correlations known to be present: collective flow, resonance decays, and momentum and charge conservation. Data cuts are applied to make track-merging effects, HBT correlations, and Coulomb effects negligible. Instrumental effects resulting from detector characteristics are accounted for in the correlation function. What remains are correlations whose origins are as yet unclear, and these are the main topic of this paper. We present high statistical precision correlations which can provide a quantitative test of the bubble model [8] and other quantitative substructure models that may be developed. We also address possible jet phenomena. These precision data could stimulate other new physics ideas as possible explanations of the observed correlations.

This paper is organized as follows. Section II describes the data utilized and its analysis. Section III describes finding a parameter set that fits the data well. Section IV presents and discusses the charge-dependent (CD) and charge-independent (CI) signals. Section V presents and discusses net charge fluctuation suppression. Section VI discusses the systematic errors. Section VII is a discussion section. Section VIII contains the summary and conclusions. Appendices provide explanatory details.

II. DATA ANALYSIS

A. Data utilized

The data reported here comprise the full sample of STAR events taken at RHIC during the 2001 running period for central Au+Au collisions at $\sqrt{s_{NN}} = 200$ GeV. The data were taken using a central trigger with the full STAR magnetic field (0.5 Tesla).

The central trigger requires a small signal, coincident in time, in each of two zero degree calorimeters, which are positioned so as to intercept spectator neutrons, and it also requires a large number of counters in the central trigger barrel to fire. Approximately 90% of the events are in the top 10% of the minimum bias multiplicity distribution, which is called the 0–10% centrality region. About 5% are in the 10–12% centrality region, with the remainder mostly in the 12–15% centrality region. To investigate the sensitivity of our analyses to the centrality of the data sample fitted, we compared fits of the entire data sample to fits of the data in the 5–10% centrality region. Both sets of fits had consistent signals within errors. Thus, no significant sensitivity to the centrality was observed in the correlation data from the central triggers.

About half the data were taken with the magnetic field parallel to the beam axis direction (z) and the other half in the reverse field direction in order to determine if directional biases are present. As discussed later in this section, our χ^2 analyses demonstrated there was no evidence of any difference in the data samples from the two field directions, and thus no evidence for directional biases.

The track reconstruction for each field direction was done using the same reconstruction program. Tracks were required to have at least 23 hits in the time projection chamber (TPC), which for STAR eliminates split tracks, and to have pseudorapidity η between -1 and 1. Each event was required to have at least 100 primary tracks. These tracks are consistent with the criteria that they are produced by a Au+Au beam-beam interaction. This cut rarely removed events. The surviving events totaled 833 000 for the forward field and 1.1 million for the reverse field. The transverse momentum selection $0.8 < p_t < 2.0$ GeV/c was then applied.

Based on the z (beam axis) position of the primary vertex, the events were sorted into ten 5 cm wide bins covering -25 to $+25$ cm. The events for the same z bin, thus the same acceptance, were then merged to produce 20 files, one for each z bin for each sign of the magnetic field.

The files were analyzed in two-dimensional (2-D) histograms of the difference in η ($\Delta\eta$), and the difference in ϕ ($\Delta\phi$) for all the track pairs in each event. Each 2-D histogram had 72 $\Delta\phi$ bins (5°) from $-180°$ to 180° and 38 $\Delta\eta$ bins (0.1) from -1.9 to 1.9. The sign of the difference variable was chosen by labeling the positively charged track as the first of the pair for the unlike-sign charged pairs, and the larger p_t track as the first for the like-sign charged pairs. Our labeling of the order of the tracks in a pair allows us to range over four $\Delta\phi\Delta\eta$ quadrants and to investigate possible asymmetric systematic errors due to space, magnetic field direction, behavior of oppositely charged tracks, and systematic errors dependent on p_t. Our consistently satisfactory results for our extensive χ^2 tests of these quadrants for fits to these precision data revealed no evidence for such effects.

Then we compared the $\Delta\phi\Delta\eta$ data for the two field directions on a bin-by-bin basis. In the reverse field data, we reversed the track curvature due to the change in the field direction, and changed the sign of the z axis, thereby making the magnetic field be in the same direction as the positive z direction. This is done by reflecting along the z axis, and simultaneously reflecting along the y axis. In the 2-D $\Delta\phi\Delta\eta$ space, this transformation is equivalent to a reflection in $\Delta\phi$ and $\Delta\eta$. For each pair, we changed the sign of its $\Delta\phi$ and $\Delta\eta$ in the reverse field data. We then calculated a χ^2 based

[1] $\Delta\phi = \phi_1 - \phi_2$ and $\Delta\eta = \eta_1 - \eta_2$.

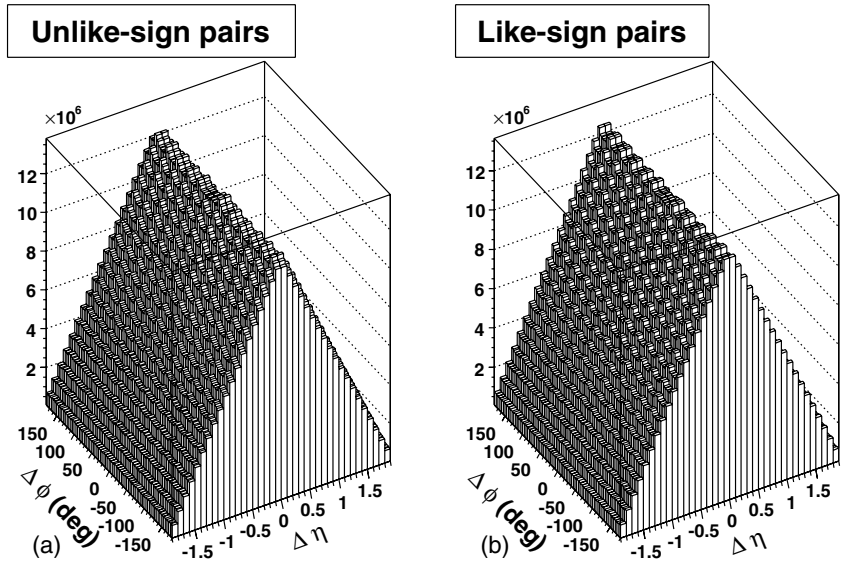

FIG. 1. $\Delta\phi\Delta\eta$ correlation data for (a) unlike-sign and (b) like-sign charged particle pairs from the STAR central trigger charged pair signal shown in 2-D perspective plots. Particle tracks have $0.8 < p_t < 2.0$ GeV/c and $|\eta| < 1.0$. The structure that looks like tiles on a roof is due to the readout boundary effects of the 12 sector TPC.

on the difference between the forward field and the reverse field, summing over the $\Delta\phi\Delta\eta$ histograms divided by the errors added in quadrature. The resulting χ^2 for the two fields showed an agreement to within 1.5σ. Therefore, we added the data for the two field directions.

We also found there was no significant dependence within 2.2σ on the vertex z coordinate. Following the same methodology, we added the files for those ten bins also.

B. Analysis method

Separate $\Delta\phi\Delta\eta$ histograms were made for unlike-sign charged pairs and like-sign charged pairs from the same-event pairs, since their characteristics were different. Both histograms were needed to later determine the CD and CI correlations as defined in Secs. IV A and IV B. These data are shown in Fig. 1. Similar histograms were made with each track paired with tracks from a different event (mixed-event pairs), adjacent in time, from the same z vertex bin. This allows use of the usual technique of dividing the histograms of the same-event pairs by the histograms of the mixed-event pairs which strongly suppresses instrumental effects such as acceptance, but leaves small residual effects. These effects include those due to the time-dependent efficiency of the tracking in the readout boundary regions between the 12 TPC sectors, which had small variations in space charge from event to event. Also, space charge in general can cause track distortion and efficiency variation event by event. The ratio of same-event pairs to mixed-event pairs histograms is shown in Fig. 2, where the plot was normalized to a mean of 1.

The expected symmetries in the data existed which allowed us to fold all four $\Delta\phi\Delta\eta$ quadrants into the one quadrant where both $\Delta\phi$ and $\Delta\eta$ were positive. After the cuts described in Sec. II C, we compared the unfolded bins to the folded average for unlike-sign charged pairs and like-sign charged pairs separately. The χ^2 were less than the degrees of freedom (DOF), and the χ^2/DOF were within 2–3σ of 1.

Thus, though we searched carefully in a number of ways to find asymmetries in the data via extensive χ^2 analyses and

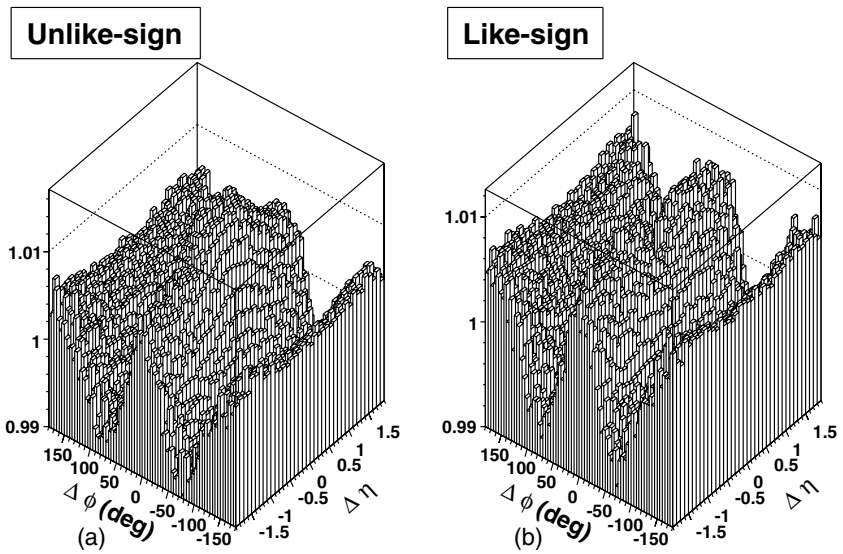

FIG. 2. Correlation data for ratio of histograms of same-event pairs to mixed-event pairs for (a) unlike-sign and (b) like-sign charged pairs, shown in 2-D perspective plots $\Delta\phi$-$\Delta\eta$. The plot was normalized to a mean of 1.

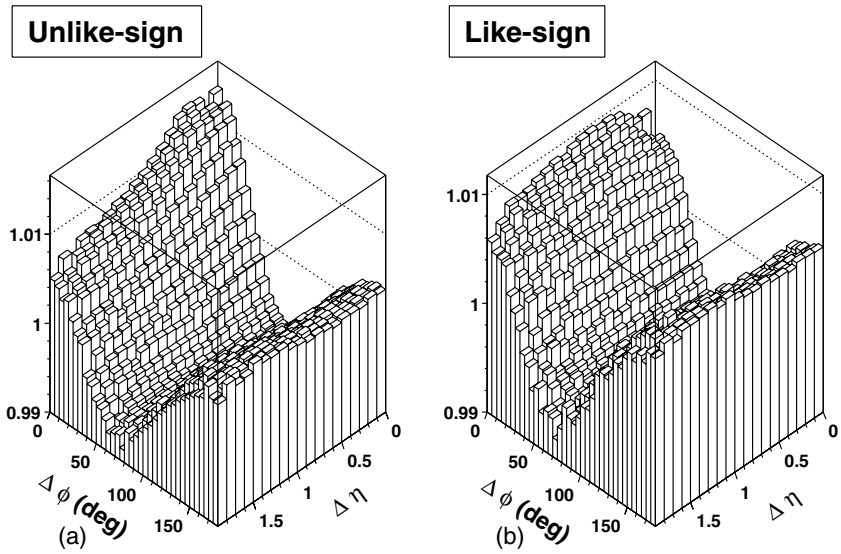

FIG. 3. Folded correlation data for (a) unlike-sign and (b) like-sign charged pairs on $\Delta\phi$ and $\Delta\eta$ based on demonstrated symmetries in the data. This increases the statistics in a typical bin by a factor of 4. Henceforth, we will be dealing with folded data only.

observation of fit behavior, none of any significance were found. By folding four quadrants into one, we quadrupled the statistics in each bin analyzed. Figure 3 shows this folded data after cuts were made (see Sec. II C) to make track-merging, Coulomb, and HBT effects negligible. Henceforth, the folded and cut data will be used for our fits.

C. Cuts

At small $\Delta\phi$ and small $\Delta\eta$ (i.e., small space angles), track-merging effects occur. To determine the cuts needed to reduce these effects to a negligible level, we varied small $\Delta\phi$ and small $\Delta\eta$ cuts. Simultaneously, the χ^2 of an approximate fit to the data using Eqs. (3), (4), and (5) was studied as a function of the bins included in the fit. With larger cuts, the χ^2 behaved properly until one or more of the cut-out bins were included in the fit. This caused a huge increase in χ^2, revealing that those bins were distorted by merging effects. We confirmed by visual inspection that track-merging effects clearly became important in the cut-out bins. The track merging caused a substantial reduction in track recognition efficiency and supported the quantitative results of our χ^2 analysis. The sharp sensitivity of the χ^2 to the cuts showed how localized the merging losses were. We adopted these cuts, and they are included in the folded data analyzed

For the unlike-sign charged pairs, we cut out the data from the regions $0.0 < \Delta\eta < 0.1$ when $0^\circ < \Delta\phi < 20^\circ$, and $0.1 < \Delta\eta < 0.2$ when $0^\circ < \Delta\phi < 10^\circ$. These cuts to make track-merging effects negligible also made the Coulomb effect negligible, since it is effective within a Δp of 30 MeV/c. This corresponds to a 2° opening angle at p_t of 0.8 GeV/c. The 2° along the beam axis near 90° corresponds to a $\Delta\eta$ of 0.035.

For the like-sign charged pairs, we cut out the data from the region $0.0 < \Delta\eta < 0.2$ when $0^\circ < \Delta\phi < 5^\circ$. The HBT effect is already small because of track merging within a Δp of 50 MeV/c, corresponding to a 4° opening angle at 0.8 GeV/c. The 4° along the beam corresponds to a $\Delta\eta$ of 0.07. All the cuts described above were also applied to the mixed events. Thus, the final track-merging cuts selected reduce the tracking problems due to overlap and merging to negligible levels; they also reduce Coulomb and HBT effects to negligible levels.

The fits to the subsequently shown data were made over the whole $\Delta\phi$ range. The data for $|\Delta\eta| > 1.5$ were cut out, since the statistics were low (see Fig. 1) and tracking efficiency varies at higher $|\Delta\eta|$.

III. PARAMETRIZATION OF DATA

We want to obtain a set of functions that will fit the data well and are interpretable, to the greatest extent practicable. We utilized parametrizations representing known, expected physics, or attributable to instrumentation effects. Any remaining terms required to obtain good fits to the data were considered as signals of new physical effects. Thus signal $\equiv$ data – (known and expected) effects. The three known effects—elliptic flow, residual instrumental effects, and momentum and charge conservation terms—were parametrized. We then found parameters for the signal terms necessary to achieve a good fit to our high statistical precision data.

In the following, we discuss the relative importance of the effects which are determined by χ^2 in our final overall fit to Eqs. (3)–(5).

A. Elliptic flow

Elliptic flow is a significant contributor to two-particle correlations in heavy ion collisions, and it must be accounted for in our analysis. Elliptic flow is not a significant contributor to two-particle correlations in pp collisions. The elliptic flow for STAR Au+Au data has been investigated in an extensive series of measurements and analyses [11] using four-particle cumulant methods and two-particle correlations. This determines a range of amplitudes (v_2) for $\cos(2\,\Delta\phi)$ terms between the four-particle cumulant that is the lower flow range boundary of $v_2(v_2 = 0.035)$ and the average value of the four- and two-particle cumulant that is the upper range boundary of $v_2(v_2 = 0.047)$. These results were determined for the

p_t range 0.8–2 GeV/c by weighting the central trigger spectrum as a function of multiplicity and centrality compared with the minimum bias trigger data for which the v_2 was measured.

The constraint is used in the following way. We find our best fit to the data by allowing the parameters in the fit to vary freely until the χ^2 is minimized. However, there is in the case of the v_2 parameter the constraint that it must lie in the flow range cited above. Since our best fit was consistent with the bottom of the flow range, it was not affected by this constraint. The value of v_2 cannot be varied to lower values because of the constraint, and thus our best fit corresponds to the lower boundary of the flow range and had a v_2 of 0.035. However, v_2 can be varied to higher values until either we reach the upper boundary or the fit worsens by 1σ, which is a χ^2 change of 32. As discussed in Sec. VI, our fit worsens by 1σ when v_2 is increased to 0.042, well within the flow range 0.035–0.047. This represents a systematic error due to flow and is the dominant error (see Sec. VI). Appendix A gives a detailed description of multiparameter fitting and error range determinations.

B. Instrumental effects

In addition to the tracking losses resulting from overlapping tracks in the TPC, which we handled by cuts, there are tracks lost in the boundary areas of the TPC between the 12 sectors. These regions result in a loss of acceptance in the ϕ measurements since the particle tracks cannot be read out by electronics. This produces a ϕ dependence with a period of 30° which is greatly reduced from about a 4% amplitude to about 0.02% (reduction by a factor of 200), by the normalization to mixed-event pairs. However, it is not completely eliminated, since STAR still has small time-dependent variations from event to event, such as space charge effects and slight differences in detector and beam behavior. To correct for the residual readout $\Delta\phi$ dependence, a term with a 30° period to represent the TPC boundary periodicity and a first harmonic term with a 60° period were used. The unlike-sign and like-sign charged pairs behave differently over the TPC boundary regions in ϕ, because positive tracks are rotated in one direction and negative tracks are rotated in the opposite direction. This requires that the sector terms have an independent phase associated with each. In Tables I and II, the terms are labeled "sector" and "sector2," "phase" and "phase2." The functional form for these sector effects is

$$\text{Sectors}\,(\Delta\phi) = S\sin(12\Delta\phi - \varphi) + S_2\sin(6\Delta\phi - \varphi_2). \quad (1)$$

There is a ϕ-independent effect which we attribute to losses in the larger η tracking in the TPC. We utilized mixed-event pairs with a similar z vertex to take into account these losses. Imperfections in this procedure leave a small bump near $\Delta\eta = 1.15$ to be represented in the fit by the terms labeled "$\Delta\eta$ bump amp" and "$\Delta\eta$ bump width" in the tables. The width of this bump should be independent of the charge of the tracks, so we constrained it to be the same for like- and unlike-sign charged pairs to improve the fit stability. Thus , the functional form for this instrumental effect is

$$\text{Etabump}\,(\Delta\eta) = Ee^{-(\Delta\eta-1.15)^2/2\sigma_E^2}. \quad (2)$$

TABLE I. Unlike-sign charged pair fit parameters for Eqs. (3) and (4). The table has three sections: Top section lists parameter names, values, and errors for the approximate Gaussian signal fit (lump). Fourth(f) is the additional term in the exponent. The source of the above is Sec. III E. The upper error is the change in each parameter when one increases the elliptic flow until the fit is 1σ worse. The lower error is determined by varying each parameter at the lower range of the elliptic flow while all the other parameters are free to readjust until the fit loses 1σ in significance. Middle section has the normalization and a small background term followed by six momentum and charge conservation terms. Source is Sec. III C. Bottom section has instrumental terms. Four terms due to TPC sector gaps and two due to large η tracking errors. Source is Sec. III B. Uncertainties are dominantly systematic, assessed as described in Appendix A.

Parameter	Value
Lump amplitude (A_u)	$0.02426^{-0.00498}_{+0.00048}$
Lump $\Delta\phi$ width ($\sigma_{\Delta\phi}$)	$32.68^{-2.12}_{+0.79}$
Lump $\Delta\eta$ width ($\sigma_{\Delta\eta}$)	$1.058^{-0.137}_{+0.065}$
Fourth (f)	$0.100^{+0.031}_{-0.028}$
Constant (B_{00})	$0.99497^{+0.00142}_{-0.00021}$
$\Delta\eta^2$ (B_{02})	0.00078 ∓ 0.00018
$\cos\Delta\phi$ (B_{10})	$-0.00710^{+0.00230}_{-0.00035}$
$\Delta\eta\cos\Delta\phi$ (B_{11})	0.00092 ∓ 0.00078
$\Delta\eta^2\cos\Delta\phi$ (B_{12})	-0.00049 ∓ 0.00057
$\cos 3\Delta\phi$ (B_{30})	$0.00058^{+0.00028}_{-0.00020}$
$\Delta\eta\cos 3\Delta\phi$ (B_{31})	0.00030 ± 0.00062
$\Delta\eta^2\cos 3\Delta\phi$ (B_{32})	-0.00014 ∓ 0.00044
Sector (S)	0.00016 ± 0.00006
Phase (φ)	8.6 ± 2.1
Sector 2 (S_2)	0.00006 ± 0.00007
Phase 2 (φ_2)	23.0 ± 10.0
$\Delta\eta$ bump amp (E)	0.00030 ∓ 0.00025
$\Delta\eta$ bump width (σ_E)	0.189 (fixed)
χ^2/DOF	572/517

In our final 3σ fits for the combined like- and unlike-sign charged pairs (see Tables I and II), leaving out the instrumental corrections would cause our 3σ fit to deteriorate to a 16σ fit, which is unacceptable. It should be noted that standard χ^2 analyses are often not considered credible if the fit exceeds 2–3σ statistical significance.

C. Correlations associated with momentum and charge conservation

It is important to ensure that momentum and charge conservation correlation requirements are satisfied. For random emission of single particles with transverse momentum conservation globally imposed, a negative $\cos(\Delta\phi)$ term alone

TABLE II. Same as Table I, but for like-sign charged pairs. Top section lists parameter names, values, and errors for the primary Gaussian signal fit (lump). This is followed by a much smaller Gaussian (dip). The rest is as described for Table II.

Parameter	Value
Lump amplitude (A_l)	$0.01823^{-0.00482}_{+0.00069}$
Lump $\Delta\phi$ width ($\sigma_{\Delta\phi l}$)	$32.02^{-2.91}_{+1.02}$
Lump $\Delta\eta$ width ($\sigma_{\Delta\eta l}$)	$1.847^{-0.315}_{+0.220}$
Dip amplitude (A_d)	$-0.00451^{-0.00092}_{+0.00090}$
Dip $\Delta\phi$ width ($\sigma_{\Delta\phi d}$)	$14.23^{-2.64}_{+2.91}$
Dip $\Delta\eta$ width ($\sigma_{\Delta\eta d}$)	$0.228^{+0.050}_{-0.041}$
Constant (B_{00})	$0.99581^{+0.00136}_{-0.00019}$
$\Delta\eta^2$ (B_{02})	$0.00100\mp.00017$
$\cos\Delta\phi$ (B_{10})	$-0.00737^{-0.00221}_{-0.00040}$
$\Delta\eta\cos\Delta\phi$ (B_{11})	$0.00075^{+0.00072}_{-0.00073}$
$\Delta\eta^2\cos\Delta\phi$ (B_{12})	$-0.00015^{-0.00054}_{+0.00055}$
$\cos 3\Delta\phi$ (B_{30})	$0.00070^{+0.00033}_{-0.00020}$
$\Delta\eta\cos 3\Delta\phi$ (B_{31})	$-0.00027^{-0.00064}_{+0.00065}$
$\Delta\eta^2\cos 3\Delta\phi$ (B_{32})	$0.00026^{+0.00044}_{-0.00045}$
Sector (S)	0.00021 ± 0.00006
Phase (φ)	22.6 ∓ 1.5
Sector2 (S_2)	0.00007 ± 0.00007
Phase2 (φ_2)	32.8 ∓ 7.0
$\Delta\eta$bump amp (E)	$0.00022^{+0.00024}_{-0.00022}$
$\Delta\eta$bump width (σ_E)	0.189 (fixed)
χ^2/DOF	588 / 519

can represent this effect. However, the complex correlations that occur at RHIC result in multiple uncorrelated sources which are presently not understood. It was not possible to fit our data with the $\cos(\Delta\phi)$ term alone. This fit was rejected by 100σ. This was not surprising since random emission of single particles with momentum conservation would not lead to the particle correlations observed at RHIC. Therefore, we suspected that a more complete description of the momentum and charge conservation was required. No one has succeeded in solving this complex problem in closed form even in the theoretical case where you observe all particles. Hence, a reasonable approach was to try to solve it for the tracks we are observing in order to obtain a good fit. We used Fourier expansion in the two variables we have, namely, $\Delta\phi$ and $\Delta\eta$.

Assuming that the $\cos(\Delta\phi)$ term for random single-particle emission was the first term in a Fourier expansion of odd terms, a second term $\cos(3\Delta\phi)$ was added and found to account for about 95% of the 100σ rejection. Based on the residual analysis, we concluded the remaining 5% required $\Delta\eta$-dependent terms for its removal. Therefore, we multiplied terms of the type $\cos(\Delta\phi)$ and $\cos(3\Delta\phi)$ by a $\Delta\eta$-dependent polynomial expansion cutting off at $\Delta\eta^2$. This essentially removed the remaining 5% rejection.

Some of the $\Delta\eta$-dependent terms make quite small contributions in the fits, but in the aggregate they improve our overall fit by about 4σ. Thus, a good fit of 3σ is downgraded to an unacceptable one of 7σ without the $\Delta\eta$-dependent expansion, since they add. One should note that fits exceeding 3σ are often not considered credible by experienced practitioners of precision data analysis, and a precision data analysis was a prime objective of this paper. In addition, we found that we needed an overall $\Delta\eta^2$-dependent fit parameter.

Summing the terms we have in Secs. III A–III C, we obtain

$$\begin{aligned}\mathbf{Bk} &= (\text{Known} + \text{Expected})\text{Effects}\\ &= B_{00} + B_{02}\Delta\eta^2 + B_{10}\cos\Delta\phi + B_{11}\Delta\eta\cos\Delta\phi\\ &\quad + B_{12}\Delta\eta^2\cos\Delta\phi + 2v_2^2\cos(2\Delta\phi) + B_{30}\cos(3\Delta\phi)\\ &\quad + B_{31}\Delta\eta\cos(3\Delta\phi) + B_{32}\Delta\eta^2\cos(3\Delta\phi)\\ &\quad + \text{Sectors}\,(\Delta\phi) + \text{Etabump}\,(\Delta\eta) \qquad (3)\end{aligned}$$

D. Fitting with Bk

We used the well-known result [12] that for a large number of degrees of freedom (DOF), where the number of parameters is a small fraction of DOF and the statistics are high, the χ^2 distribution is normally distributed about the DOF. The significance of the fit decreases by 1σ whenever the χ^2 increase is equal to $\sqrt{2(\text{DOF})}$, which for our 517–519 DOF is equal to 32. Appendix A gives further details.

If we fit the functional form of **Bk** [Eq. (3)] to both the unlike- and like-sign charged pairs, i.e., the whole data set, χ^2 is about 10 400 for about 1045 DOF.

The standard deviation on 1045 DOF is about 46, so the fit is rejected by around 200σ. We used many free parameters (15) in Eq. (3), yet additional unknown terms appear to be so sharply varying that it is clearly impossible for the **Bk** functional form to fit the data. A more detailed discussion of the statistical methods used in the data analyses and the treatment of systematic and other errors in this paper is given in Appendix A.

E. Signal terms

Many signal terms in physics are Gaussian-like. We therefore tried fitting the signal data using 2-D Gaussians or approximate Gaussians. The unlike-sign charged pair correlations were well fit (2σ) by adding to **Bk** an additional 2-D approximate Gaussian in $\Delta\eta$ and $\Delta\phi$ [Fig. 4(a)] given by

$$\text{Unlike} - \text{sign Signal} = A_u e^{-(\Delta\phi^2/2\sigma_\phi^2 + \Delta\eta^2/2\sigma_\eta^2 - f\Delta\eta^4)}. \qquad (4)$$

Considering the enormous improvement in fit quality afforded by the addition of this signal term, we conclude that this function in Eq. (4) provides a compact analytic description of the signal component of the unlike-sign charged pair correlation data. The fit was improved by the addition of a term dependent on $\Delta\eta^4$ in the exponent (called "fourth" in Table I). The fit for the unlike-sign charged pair signal data is shown in Fig. 4(a). The unlike-sign charged pair signal data corresponding to the fit (unlike-sign charged pair data minus **Bk**) is shown in Fig. 4(b).

The like-sign charged pair data, which also could not be fit by **Bk** alone, were well described (2σ) when we added [see

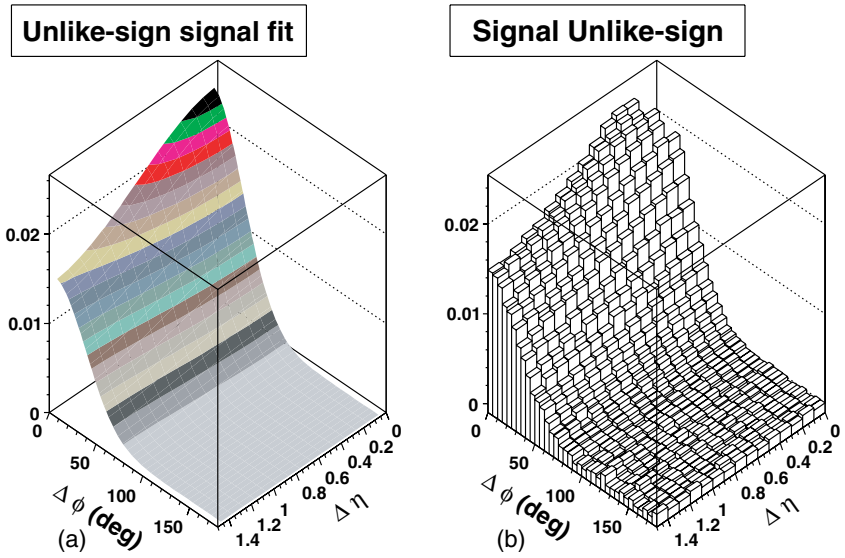

FIG. 4. (Color online) (a) 2-D approximately Gaussian signal shape of Eq. (4) from the fit to the normalized and folded unlike-sign charged pair signal data. (b) Unlike-sign charged pair signal data corresponding to the adjoining signal function in (a).

Fig. 3(b)] a positive 2-D Gaussian and a small negative 2-D Gaussian dip given by

$$\text{Like} - \text{sign Signal} = A_l e^{-(\Delta\phi^2/2\sigma_{\phi l}^2 + \Delta\eta^2/2\sigma_{\eta l}^2)} + A_d e^{-(\Delta\phi^2/2\sigma_{\phi d}^2 + \Delta\eta^2/2\sigma_{\eta d}^2)}. \quad (5)$$

Therefore, we conclude that Eq. (5) provides an efficient description of the signal component of the like-sign charged pair data. The large signal referred to in Table II as "lump" in the like-sign charged pair correlation is a 2-D Gaussian centered at the origin. It is accompanied by a small narrower 2-D Gaussian "dip" (also centered at the origin) subtracted from it. The terms are labeled in the fits as lump amplitude, dip amplitude, lump $\Delta\phi$ width, lump $\Delta\eta$ width, dip $\Delta\phi$ width, and dip $\Delta\eta$ width. Note that the volume of the dip is about 1.6% of the volume of the large lump signal. However, if we neglect to include this small dip, our fit deteriorates by 28σ. This dip might be caused by suppression of like-sign charged particle pair emission from localized neutral sources such as gluons. The function fit to the like-sign charged pair signal data is shown in Fig. 5(a). The like-sign charged pair signal data (like-sign charged pair data minus **Bk**) is shown in Fig. 5(b). The uncertainties quoted throughout this paper correspond to a change in χ^2 of $\Delta\chi^2 = 32$, rather than the more commonly used $\Delta\chi^2 = 1$ (see Appendix A for more details).

F. Summary of parametrizations

Equations (3) + (4) yield a 2σ fit for the unlike-sign charged pair correlation, and thus is an appropriate and sufficient parameter set.

Equations (3) + (5) yield a 2σ fit for the like-sign charged pair correlation, and thus is an appropriate and sufficient parameter set.

Equations (3) + (4) + (5) yield a 3σ fit for the entire data set, unlike-sign charged pair correlation + like-sign charged pair correlation, and thus is an appropriate and sufficient parameter set for the entire data set.

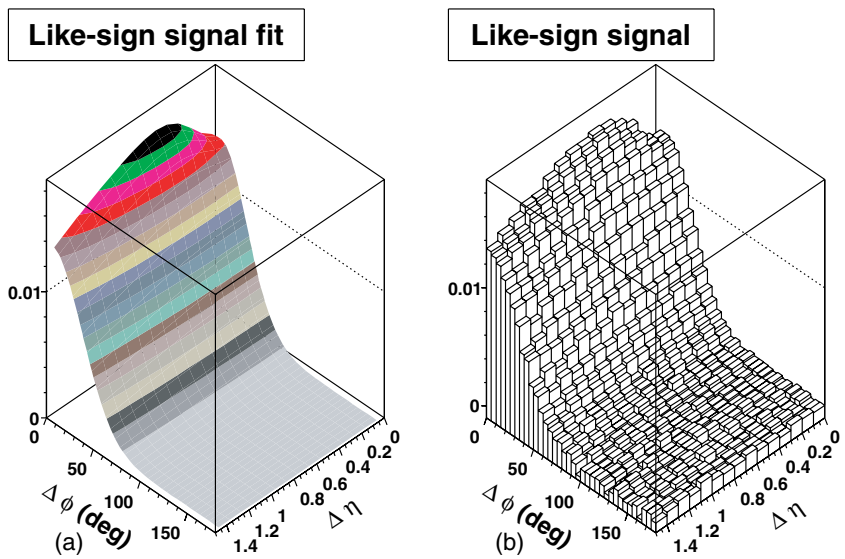

FIG. 5. (Color online) (a) Perspective plot of fit to 2-D like-sign charged pair signal shape of Eq. (5). (b) Like-sign charged pair signal data corresponding to the adjacent signal fit in (a).

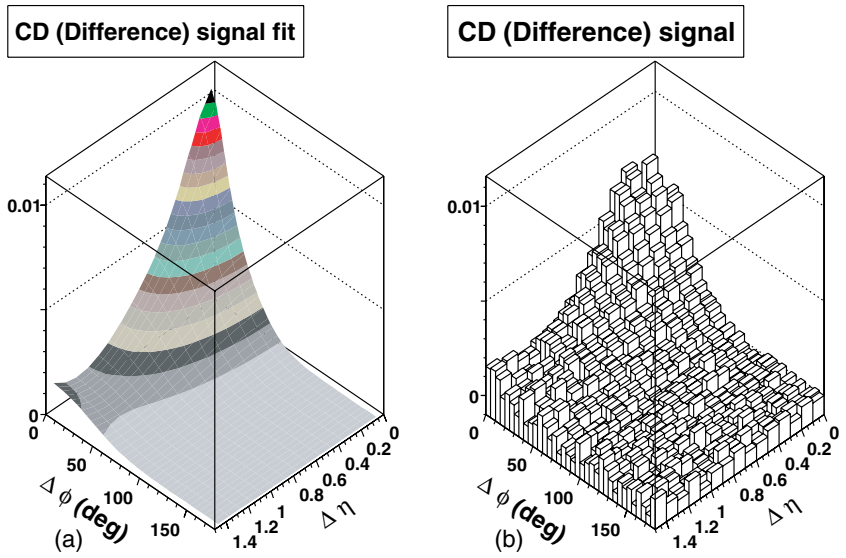

FIG. 6. (Color online) (a) CD signal shape is a 2-D approximate Gaussian which is symmetrical. Average Gaussian width is $27.5^\circ \pm 3.2^\circ$ (0.48 ± 0.056 rad) both in $\Delta\phi$ and $\Delta\eta$. Thus we are observing a greater probability for unlike-sign charged pairs of particles than for like-sign charged pairs emitted randomly on 2-D $\eta\phi$ directions. (b) CD signal data corresponding to the adjacent signal fit in (a).

The complex multidimensional χ^2 surface makes χ^2 increase nonlinearly with the number of error ranges (1σ) given in Tables I and II. Therefore, in order to determine the significance of a parameter or group of parameters, one must fit without them and determine by how many σ the fit has worsened. Then, one uses the normal distribution curve to determine the significance of the omitted parameter(s). The results of such an investigation were

(i) Leave out $\cos(3\Delta\phi)$ and the fit worsens by 95σ.
(ii) Leave out dip and the fit worsens by 28σ.
(iii) Leave out sector terms and the fit worsens by 11.7σ.
(iv) Leave out η-dependent $\cos(\Delta\phi)$ and $\cos(3\Delta\phi)$ terms and the fit worsens by 4.3σ.
(v) Leave out η bump terms and the fit worsens by 1.54σ.
(vi) Leave out sector 2 and the fit worsens by 1.41σ.

Since our global fit with all the above terms is at the 3σ level, we conclude that the above terms are necessary. The huge number of σ we get for some of the parameters are only to be taken as a qualitative indication of the need for the parameters to fit our high precision data. Because of the uncertainties in determining the number of σ far out on the tails of the normal distribution (i.e., $> 10\sigma$), a quantitative interpretation of them cannot be made.

IV. CD AND CI SIGNALS

A. Charge-dependent (CD) signal

If we subtract the entire like-sign charged pair correlation [Eq. (5)] from the unlike-sign charged pair correlation [Eq. (4)], we obtain the CD correlation. However, it is observed that the backgrounds (**Bk**) of the two terms are close enough in value to cancel each other in the subtraction. Thus the CD signal is essentially the same as the entire CD correlation. In the extensive study of the balance function [13] for the correlation due to unlike-sign charged pairs which are emitted from the same space and time region, it is argued that the emission correlation of these pairs can be approximately estimated from the balance function. The balance function for these charged pairs is proportional to the unlike-sign charged pairs minus the like-sign charged pairs. Therefore, the CD signal which is approximately equal to the CD correlation is a qualitative measure of the emission correlation of unlike-sign charged pairs emitted from the same space and time region. In addition to the approximations involved in the balance function, there is the modification to the CD signal discussed in Sec. IV D.

Figure 6(a) shows the fit to the CD signal; Fig. 6(b) shows the CD signal data that were fit. The signal form is a simple Gaussian in both $\Delta\phi$ and $\Delta\eta$. The Gaussian width in $\Delta\phi$ is $28.3^\circ \pm 3.4^\circ$ (0.49 ± 0.059 rad), and the Gaussian $\Delta\eta$ width is 0.485 ± 0.054. Converting this pseudorapidity to a θ angle yields a width of $26.7^\circ \pm 3.0^\circ$ (0.47 ± 0.052 rad). This correlation has the same angular range in $\Delta\eta$ and $\Delta\phi$. Therefore, we observe pairs of oppositely charged particles emitted randomly in the η and ϕ direction with a correlation which has an average Gaussian width of about $27.5^\circ \pm 3.2^\circ$ (0.48 ± 0.056 rad) in the θ angle corresponding to $\Delta\eta$ and also in the azimuth $\Delta\phi$.

B. Charge-independent (CI) signal

If we add the like-sign charged pair signal to the unlike-sign charged pair signal, we obtain the CI signal. The CI signal fit shown in Fig. 7(a) displays the average structure of the correlated emitting sources. Figure 7(b) shows the CI signal data that were fit by the analytic distribution shown in Fig. 7(a).

To obtain a good fit to the shape, both in $\Delta\eta$ and $\Delta\phi$, we needed a more complicated form than one simple 2-D Gaussian. The CI signal actually contains an approximate Gaussian from the unlike-sign charged pair signal plus two Gaussians from the like-sign charged pair signal.

We want to obtain a measure of the effective $\Delta\phi$ and $\Delta\eta$ widths of the overall pattern of the CI signal. A good method for doing this is to compare the CI signal with a single Gaussian which yields the same rms values as the actual good fit described above involving two Gaussians and an approximate Gaussian. For $\Delta\phi$, that σ is $32.0^\circ \pm 0.6^\circ$($0.56 \pm$

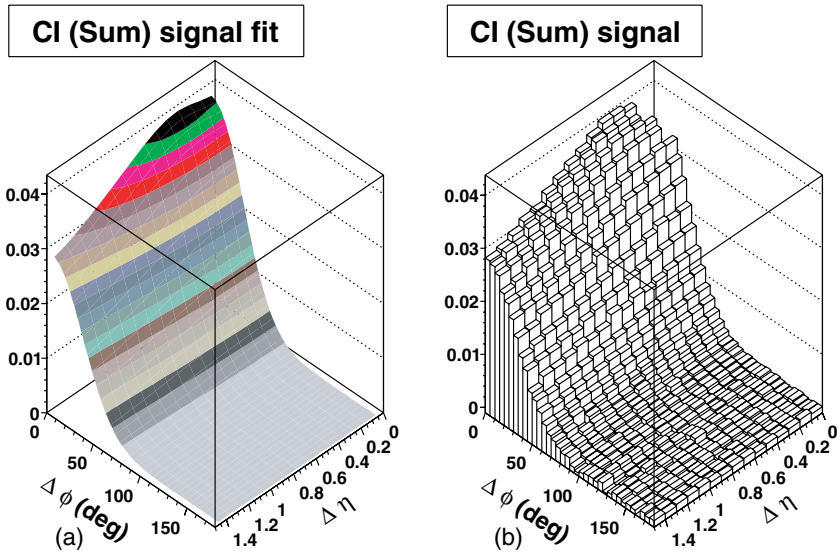

FIG. 7. (Color online) (a) Fit to CI signal shape which is the sum of the fits of like-sign plus unlike-sign charged pair signals. The 2-D Gaussian equivalent rms signal has a $\Delta\phi$ width of about 32° (0.52 rad), and $\Delta\eta$ width of about 66°(1.15 rad) which is about double the $\Delta\phi$ width. (b) CI signal data corresponding to the adjacent fit in (a).

0.01 rad). For $\Delta\eta$, that σ is 1.55 corresponding to an angle of $66.0^{\circ}{}^{+1.0^{\circ}}_{-0.6^{\circ}}$(1.15 ± 0.02 rad). Thus, the correlation is about twice as wide in $\Delta\theta$, the angle corresponding to $\Delta\eta$, than in the angle corresponding to $\Delta\phi$ [see Fig. 7(a)].

Another STAR measurement reports CD and CI correlations at $\sqrt{s_{NN}} = 130$ GeV/c [14].[2] The major differences between that previous analysis and the present work are the larger range in p_t $0.15 < p_t < 2.0$ GeV/c and the lower statistical quality of the limited 130 GeV/c data set. Although the analysis in Ref. [14] included low p_t particles, there is reasonable qualitative agreement with the present results.

C. Resonance contribution

To determine the maximum contribution and effect resonances can have on the CI signal, we consider the following. Resonances mainly decay into two particles. Therefore, neutral resonances that decay into charged pairs could be a partial source of the unlike-sign charged pairs in CD and CI signals. However, resonances do not add significant correlation to the like-sign charged pairs in either the CD or the CI signals.

We expect that the final state particles from the resonance decay distribution will be symmetrical in the $\Delta\phi$ angle and in the angle corresponding to $\Delta\eta$ since we do not expect any polarization mechanism that would disturb this expected symmetry. The fact that in the CD both the $\Delta\phi$ angle and the angle corresponding to $\Delta\eta$ are approximately the same supports this. In this section, we evaluate the possible effects of resonance decay on the CI signal which definitely is observed to be elongated in the corresponding $\Delta\eta$ angle by about a factor of 2 compared with that in the $\Delta\phi$ angle. The CI signal is always defined as CI signal = (unlike-sign charged pair signal) + (like-sign charged pair signal). CD signal = (unlike-sign charged pair signal) − (like-sign charged pair signal). By subtracting the CD signal from the CI signal and rearranging terms in the equation, one obtains CI signal = CD signal + 2 (like-sign charged pair signal).

There is particular interest in the shape of the CI signal when comparisons are made with theoretical models, e.g., HIJING and Ref. [8]. The $\Delta\phi$ shape is about the same in the CI and CD signals. Therefore, we need only estimate the effect of resonances on the $\Delta\eta$ width. By making the extremely unrealistic assumption that the CD signal is composed entirely (100%) of resonances, we can estimate the maximum effect of resonances on the CI signal $\Delta\eta$ width. We use the equivalent Gaussian which has the same rms widths for this calculation. From the data, we determine that the $\Delta\eta$ width of the CI signal is increased by a 7% upper limit. However, if we use the result from Appendix B that the resonance content of the CD is 20% or less, we must divide the 7% by 5, which results in an increase of $\Delta\eta$ width of only about 2%. Either estimate of the $\Delta\eta$ width increase is inconsequential, compared to the observed approximate factor of 2 elongation of the $\Delta\eta$ width compared with the $\Delta\phi$ width. Details of these calculations are given in Sec. VI and Appendix B.

D. Modification of CI and CD signals

The CI and CD signals existing at the time of hadronization are changed by the continuing interaction of the particles until kinetic freeze-out, when interactions cease. The interactions are expected to reduce the signals. Therefore, we expect that the observed signals are less than those existing at the time of hadronization.

V. NET CHARGE FLUCTUATION SUPPRESSION

Net charge fluctuation suppression is an observed percentage reduction in the rms width of the distribution of the number of positive tracks minus the negative tracks plotted for each event, compared with the rms width of a random distribution.

If there are localized, uncharged bubbles of predominantly gluons in a color singlet, when the bubbles hadronize, the

[2]The CD correlation in Ref. [14] is defined as like-sign pairs minus unlike-sign charged pairs, which has an opposite algebraic sign relative to the definition used in this paper.

total charge coming from the bubbles is very close to zero. Therefore, if we are detecting an appreciable sample of such bubbles, we expect to see net charge fluctuation suppression.

It should be noted that net charge fluctuation suppression can be deduced from the CD correlation given previously. Net charge fluctuation suppression previously analyzed at lower momenta has been found consistent with resonance decay [15]. However, the present analysis has different characteristics. Furthermore, Ref. [8] has made specific estimates of net charge fluctuation suppression applicable to this experiment. We performed a charge difference analysis for tracks within cuts of $0.8 < p_t < 2.0$ GeV/c and $|\eta| < 0.75$. This would allow a comparison with Ref. [8].

For each event, we determined the difference of the positive tracks minus the negative tracks in our cuts. There was a net mean positive charge of 4.68 ± 0.009. The width of the charge difference distribution given by rms was 11.149 ± 0.017. To determine the net charge fluctuation suppression, we need to compare this width with the width of the appropriate random distribution, which would have no net charge fluctuation suppression. However, we must arrange a slight bias toward a positive charge so that we end up with the same net mean positive charge as observed. If we now assign a random charge to each track with a slight bias toward being positive such that the mean net charge is also 4.68 ± 0.009, the width (rms) becomes 11.865 ± 0.017. The percentage difference in the widths, which measures the net charge fluctuation suppression, is $6.0\% \pm 0.2\%$.

VI. SYSTEMATIC ERRORS

Systematic errors were minimized using cuts and corrections. The cuts (see Sec. II C) were large enough to make the contributions from track merging, Coulomb, and HBT effects negligible.

Systematic checks utilized χ^2 analyses which verified that the experimental results did not depend on the magnetic field direction, the vertex z coordinate, or the folding procedures (see Secs. II A and II B). By cutting the track η at 1.0, we keep the systematic errors of the track angles below about 1° [16].

In Sec. IV C, we referred to a simulation in Ref. [8], which estimated that the background resonance contribution to the CD correlation cannot be more than 20% (see Appendix B). From the resonance calculations discussed in Appendix B, the background resonance contribution to the unlike-sign charged pair correlation would be reduced to 5%. The details that justify this are the following. Our analyses measured an average of 19 unlike-sign charged signal pairs per event from the CD correlation signal. The total average number of unlike-sign charged signal pairs is 88. Therefore, with the extreme assumption that all of the CD correlation signal is due to background resonances, 21.6% of the unlike-sign charged signal pairs are due to resonances. However, as discussed in Appendix B, the estimated contribution of resonances to the CD correlation is 20% or less. Therefore, $21.6\%/5 = 4.3\%$ is the resonance content of the unlike-sign charged signal pairs, which we rounded to 5%.

We also concluded via an upper limit calculation with the above extremely unrealistic assumption that the shape of the CI signal could only have the measured width in $\Delta\eta$ increased by about 7%. This is inconsequential compared to the factor of 2 increase in $\Delta\eta$ width compared with $\Delta\phi$ width. For the simulation discussed above, in which resonance backgrounds contribute 20% to the CD correlation, the increase in the CI correlation $\Delta\eta$ width would be limited to about 2%.

The CI and CD signals are more physically significant than the unlike- and like-sign charged pair signals, since they are physically interpretable. The CI signal fit displays the average structure of the correlated emitting sources (Sec. IV B). The analysis suggests that the CD signal (Sec. IV A) is a qualitative representation of the emission correlation of the unlike-sign charged pairs emitted from the same space and time region. Elliptic flow contributions to the like- and unlike-sign charged pair signals are approximately equal and therefore cancel in the CD signal. Thus, the CD signal is not affected by uncertainty in the elliptic flow amplitude.

In Fig. 8(a) we show the CI signal data with the lower flow range value of mean elliptic flow amplitude (weighted over the p_t range of the data) used in the fit, namely, $v_2 = 0.035$. This

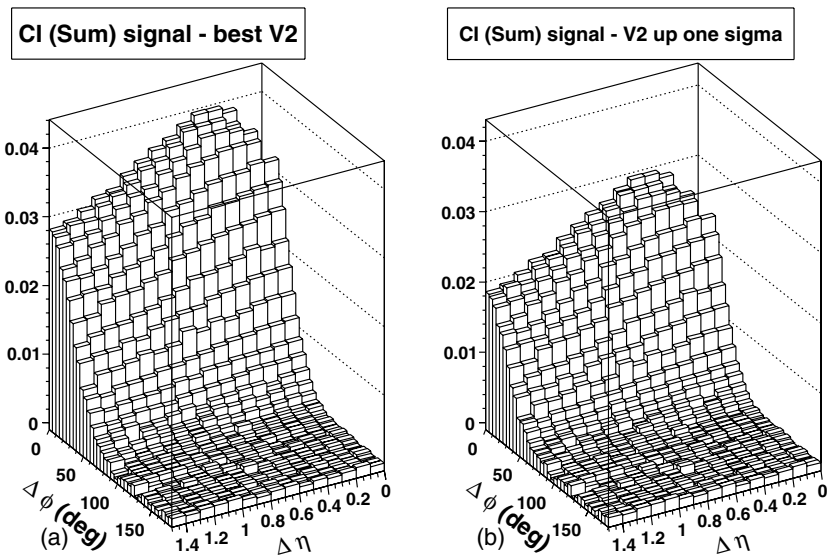

FIG. 8. (a) CI signal data with the lower range of elliptic flow amplitude and the best χ^2 [same as Fig. 7(b)] plotted as a 2-D perspective plot on $\Delta\phi$ vs $\Delta\eta$. (b) CI signal data with the maximum elliptic flow amplitude used in our analysis (χ^2 was worse by 1σ).

is our best fit, in which the value of v_2 is consistent with the lower flow range. Thus, Fig. 8(a) is the same as Fig. 7(b). In Fig. 8(b), we show the CI signal data with our maximum amount of elliptic flow allowed. This value of elliptic flow causes our fit to be 1σ worse and corresponds to a χ^2 increase of 32. This results in a mean weighted $v_2 = 0.042$. This value of elliptic flow lies in the determined flow range, but is smaller than the upper limit of 0.047 [11]. The upper error ranges in Tables I and II are determined by the effect of this change in the elliptic flow ($0.042 > v_2 > 0.035$), since it is the dominant error that results in these range values. The main change in Fig. 8(b) compared to Fig. 8(a) is that the peak amplitude is reduced by 25%, and the 2-D area is reduced by 34%. However, the most significant CI signal parameters in comparing to theoretical models are those that measure the shape, namely, the ratio of rms $\Delta\phi$ and $\Delta\eta$ widths, of a Gaussian equivalent to the fit. For our best fit, $\Delta\phi$ width $= 32.0^\circ \pm 0.6^\circ$ (0.56 ± 0.01 rad), and $\Delta\eta$ width $= 1.55$, which is equivalent to $66.0^{\circ\,+1.0^\circ}_{-0.6^\circ}$($1.15 \pm 0.02$ rad). The ratio $\Delta\eta$ equivalent angle/$\Delta\phi = 2.06$. For the case of the maximum elliptic flow value, the determined widths were $\Delta\phi = 30.1^\circ$ (0.53 rad), and $\Delta\eta = 1.375$ (61.6°or 1.08 rad). The ratio $\Delta\eta/\Delta\phi = 2.05$. Thus, the important shape ratio has changed by about 1%.

Let us now address the errors due to contamination by including secondary particles arising from weak decays and the interaction of antiprotons and other particles in the beampipe and material near the beampipe. These secondary particle backgrounds have been estimated to be about 10–15% [17]. In this analysis, we are concerned mainly with the angles of the secondary particles relative to the primaries that survive our high p_t cut, not their identity or exact momentum magnitude. Our correlations almost entirely depend on angular measurements of $\Delta\phi$ and $\Delta\eta$. In the range $0.8 < p_t < 2.0$ GeV/c, we have considered the behavior of weakly decaying particles and other nonprimary particles that could satisfy our distance of closest approach to the primary vertex and p_t cuts. Because high p_t secondary particles are focused in the same direction as the primaries, only a fraction of these particles have sufficient change in angle that would cause an appreciable error in our correlation. Hence, our estimate is a systematic error of about 4% due to secondary particles.

Next we summarize our extensive discussion of systematic errors. Track-merging errors, Coulomb, and HBT effects were made negligible by cutting out effected bins at small space angles. Instrumental errors were corrected for in the parametrization. Elliptic flow error is our dominant systematic error, because of the uncertainty that exists in the elliptic flow analyses [11]. It should be noted that the size of the upper error range of our parameter errors in Tables I and II are determined by the maximum value of the elliptic flow we allowed ($v_2 = 0.042$), which corresponds to a χ^2 change of 32 (1σ). The sizable change to the CI signal shown in Fig. 8(b) compared with that in Fig. 8(a) is due to this maximum allowed value of elliptic flow. As shown above, the shape ratio of the CI signal, which is important for theoretical comparison, is changed, fortunately, by only about 1%. When more accurate elliptic flow results become available, it will be a simple matter to insert these in the fits and reduce the resultant error. The next smaller systematic error is due to possible background resonance errors. The smallest systematic error is due to secondary contamination. As discussed above, none of these errors significantly affect our important physical conclusions.

VII. DISCUSSION

Highly significant correlations are observed for unlike-sign and like-sign charged pairs, and consequently for charge-dependent and charge-independent signals. The CD signal is well described (with a 1σ fit) by a symmetrical 2-D Gaussian with a rms width of about 30° in both $\Delta\phi$ and $\Delta\eta$. Conservative simulations in Ref. [8] indicate that the contribution to this CD signal from background resonance decay is less than 20%. Simulations (see Appendix B) estimate that the only significant change due to the background resonances is an increase in the CD amplitude of 20% or less. The CI signal is more complex and is the sum of the unlike-sign charged pair signal and the like-sign charged pair signal fits. Therefore, it contains an approximate Gaussian from the unlike-sign charged pair signal, and a large positive Gaussian plus a small negative Gaussian (dip) from the like-sign charged pair signal. The dip contains only 1.6% of the like-sign charged signal volume. This small dip, observed for the first time, has high significance in the fit. This feature is consistent with what one would expect for suppression of like-sign charged pair emission from a localized neutral source such as gluons.

A 2-D Gaussian which yields the same rms widths as our overall CI signal has a σ along the $\Delta\phi$ direction of $32.0^\circ \pm 0.6^\circ$ (0.56 ± 0.01 rad). However, the $\Delta\eta$ σ is 1.55 corresponding to an angle of approximately 66°(1.15 rad) and thus is twice as wide.

The mean charge difference for tracks within the chosen analysis cuts is 4.68 ± 0.009 net positive charges, and the rms variation of this quantity from event to event is 11.149 ± 0.017. A random charge assignment constrained to produce the same mean net charge has a larger width of 11.865 ± 0.017. The difference, $6.0\% \pm 0.2\%$, measures the net charge fluctuation suppression.

The HIJING model produces jets in our p_t range which are nearly symmetrical in $\Delta\phi$ and the angle corresponding to $\Delta\eta$ [18]. The proper way to compare our data with HIJING is to compare our CI signal with the above-mentioned HIJING CI correlation from jets. As shown in Sec. IV B, our CI signal is highly asymmetric because the angle corresponding to $\Delta\eta$ is about twice the angle $\Delta\phi$, thus it strongly contradicts these basic characteristics of HIJING jet correlations.

A detailed comparison of the STAR data presented here with a model based on a ring of localized bubbles emitting charged particles from the central fireball surface at kinetic freeze-out reported a good consistency between the STAR data and the model [19].

VIII. SUMMARY AND CONCLUSIONS

We performed an experimental investigation of particle-pair correlations in $\Delta\phi$ and $\Delta\eta$ using the main time projection

chamber of the STAR detector at RHIC. We investigated central Au+Au collisions at $\sqrt{s_{NN}} = 200$ GeV, selecting tracks having transverse momenta $0.8 < p_t < 2.0$ GeV/c and the central pseudorapidity region $|\eta| < 1.0$. The data sample consists of 2 million events, and the symmetries of the data in $\Delta\eta$ and $\Delta\phi$ allow four quadrants to be folded into one. The entire data set (unlike-sign charged pairs and like-sign charged pairs) was fit by a reasonably interpretable set of parameters, 17 for the unlike-sign charged pairs and 19 for the like-sign charged pairs. These parameters are small in number compared with the total number of degrees of freedom, which was over 500 for each of the two types of pairs. Every fit reported here using these parameters was a good fit of 2 to 3 σ or less.

From our analysis of the systematic errors, we conclude that the important features of our data and the conclusions drawn have not been significantly affected by the systematic errors.

This paper serves as an excellent vehicle for making detailed comparisons with and testing of various theoretical models such as the bubble model [8] and other relevant models.

ACKNOWLEDGMENTS

We thank the RHIC Operations Group and RCF at BNL, and the NERSC Center at LBNL for their support. This work was supported in part by the Offices of NP and HEP within the U.S. DOE Office of Science; the U.S. NSF; the BMBF of Germany; IN2P3, RA, RPL, and EMN of France; EPSRC of the United Kingdom; FAPESP of Brazil; the Russian Ministry of Science and Technology; the Ministry of Education and the NNSFC of China; IRP and GA of the Czech Republic; FOM of the Netherlands; DAE, DST, and CSIR of the Government of India; Swiss NSF; the Polish State Committee for Scientific Research; SRDA of Slovakia; and the Korea Science and Engineering Foundation.

APPENDIX A: MULTIPARAMETER FITTING IN THE LARGE DOF REGION AND SYSTEMATIC UNCERTAINTIES

Let us now consider the details of multiparameter data analysis in the large DOF region in terms of change of χ^2 for our 517–519 n for unlike-sign and like-sign charged pairs. A 1σ change in the significance of the individual fits require the change in χ^2 of 32. The reader is referred to Ref. [12] from which we quote: "For large n(DOF), the χ^2 p.d.f.(probability density function) approaches a Gaussian with mean = n and variance (σ) squared = $2n$." For $n > 50$–100, this result has been considered applicable, and it remains applicable and becomes more accurate as n increases toward infinity. Thus, for our 517–519 n, $1\sigma = \sqrt{2n} = 32$.

The statistical significance of any fit in this paper can be obtained by the following procedure. The number of σ of fit = $(\chi^2 - n)/32$. The number of σ refer to the normal distribution curve.

For large DOF(bins-parameters) fluctuations occur because of the many bins. When one fits the parameters, one will try to describe some of these fluctuations. Therefore, we need to check whether the fluctuations in the data sample are large enough to significantly distort the parameter values. This has traditionally been done by using the confidence level tables vs χ^2 which allows a reasonable determination of the fluctuations due to binning. The approximation (described above) we have used is an accurate extension of the confidence level tables.

Let us consider our method of assigning systematic error ranges to the parameters. Our objective is to obtain error ranges that are not likely to be exceeded if future independent data samples taken under similar conditions are obtained by repetition of the experiment by STAR or others. We want to avoid the confusion and uncertainty of apparent significant differences in parameters when the fit to new data does not differ significantly from a previous fit. We allow each parameter, one at a time, to be varied (increased and then decreased) in both directions while all the other parameters are free to readjust until the overall fit χ^2 degrades in significance by 1σ. This corresponds to an increase of χ^2 of 32 for the unlike-sign and like-sign charged pair fits. The χ^2 surface has been observed, and χ^2 increases very nonlinearly with small increases of the parameter beyond the error range.

When one assumes that the parameter error is given by a χ^2 change of 1 in the best fit [20], this is correct for the case where you know the underlying physics. The purpose of our use of parameters is not to determine their true values, since we do not know the underlying physics. We use the parameters to determine an analytic description of the data that fits the data within 2–3σ.

Let us address how one determines the significance of a parameter or a particular group of parameters in the case of this multiparameter analysis. It is entirely incorrect to compare the error ranges in Tables I and II with the parameter value. The only correct way to determine the significance of a parameter or group of parameters in the multiparameter fit is to leave the parameters out of the fit and refit without them. One then determines by how many σ the overall fit has degraded compared with a change of 32 for 1σ.

One should note that the upper error range on a parameter in Tables I and II represents the change in value of the parameter as we increase v_2, our dominant error, from our best fit until the fit worsens by 1σ (χ^2 increases by 32). The other parameters are free to readjust during the foregoing variation. The lower error range is the result of changing the parameter in the opposite direction of it in the upper range while the other parameters are free to readjust until the fit decreases in significance by 1σ. The largest error that dominates the upper systematic error range determination is the variation of the v_2 error. However, the constraint of v_2 to the flow range, and the fact that our best fit is at the lower end of the range, means that flow is not varied when we determine the lower error. Therefore, the elimination of the large flow variation leads to generally smaller lower error ranges and thus the observed asymmetry between the upper and lower error ranges.

Finally if one fixes any one of the parameters at the end of the error ranges with the correct v_2 assigned (0.042 upper and 0.035 lower) and lets all the other parameters readjust, one will achieve an overall fit which is only worse by 1σ (a χ^2 increase of 32).

APPENDIX B: RESONANCE CALCULATIONS

In this section, we discuss background resonances having the following meaning. Background resonances are resonances that only contribute to the unlike-sign charged pair correlation. Any resonance that is emitted as part of a correlated emitter will also have a like-sign charge correlation. This is because any of the charges will have another particle of the same charge with which to correlate that is also emitted by the correlated emitter. The background resonances we are discussing are not part of the correlated emitters we want to study, but will add to the CD correlation.

In Ref. [8], a table of resonances and particles was considered in a thermal resonance gas model. The resonance content was adjusted to cause the 20% net charge fluctuation suppression observed at lower momentum in a STAR experiment for central Au+Au collisions. The result of this model calculation is a 20% contribution of resonances to the CD correlation. The p_t range of the analysis $0.8 < p_t < 2.0\,\mathrm{GeV}/c$ tends to have the symmetric pairs of particles from resonance production decay into angles within the range of our cuts. However, asymmetric decays only contribute one particle of the pair and thus do not add to the correlation. Therefore, effectively, only a part of the estimated resonance contribution affects the correlation measurement. Our simulations reveal that the only significant change that the background resonance contribution would introduce into the CD correlation is an increase in amplitude of 20% or less. The CI signal = CD signal + 2(like-sign charged pair signal). The resonance contribution to the like-sign charged pair signal is small. The affect of resonances on the CI signal elongation in the $\Delta\eta$ width is estimated by the model simulation to be a factor of 5 lower than the extreme maximum case previously assumed, namely, that the entire CD correlation is composed of background resonances. Thus, this would result in a $\Delta\eta$ width elongation of the CI signal of approximately 2% instead of the upper limit of 7%.

[1] J. Adams *et al.* (STAR Collaboration), Nucl. Phys. **A757**, 102 (2005).

[2] For an overview, see *Quark Matter Formation and Heavy Ion Collisions, Proceedings Biefield Workshop (May 82), Quark Matter 2004,* J. Phys. G **30**, s633 (2004).

[3] Special Issue: The Relativistic Heavy Ion Collider Project RHIC and Its Detectors, Nucl. Instrum. Methods A **499**, 235 (2003).

[4] J. Adams *et al.* (STAR Collaboration), Phys. Rev. C **70**, 054907 (2004).

[5] F. Karsch, Nucl. Phys. **A698**, 199c (2002).

[6] L. Van Hove, Hadronization Quark-Gluon Plasma in Ultra-Relativistic Collisions, CERN-TH (1984) 3924; L. Van Hove, Z. Phys. C **27**, 135 (1985).

[7] S. J. Lindenbaum and R. S. Longacre, J. Phys. G **26**, 937 (2000). This paper contains earlier (1985 onward) references by these authors.

[8] S. J. Lindenbaum, R. S. Longacre, and M. Kramer, Eur. Phys. J. C **30**, 241 (2003).

[9] J. Adams *et al.* (STAR Collaboration), Phys. Rev. C **71**, 044906 (2005); S. S. Adler *et al.* (PHENIX Collaboration), Phys. Rev. Lett. **93**, 152302 (2004).

[10] C. Adler *et al.*, Nucl. Instrum. Meth. A **499**, 433 (2003); K. H. Ackermann *et al.*, *ibid.* **499**, 624 (2003); M. Anderson *et al.*, *ibid.* **499**, 659 (2003); F. S. Bieser *et al.*, *ibid.* **499**, 766 (2003).

[11] K. H. Ackerman *et al.* (STAR Collaboration), Phys. Rev. Lett. **86**, 402 (2001); C. Adler *et al.* (STAR Collaboration), *ibid.* **90**, 032301 (2003); J. Adams *et al.* (STAR Collaboration), Phys. Rev. C **72**, 014904 (2005).

[12] S. Eidelman *et al.*, Phys. Lett. **B592**, 1 (2004), see p. 278.

[13] S. A. Bass, P. Danielewicz, and S. Pratt, Phys. Rev. Lett. **85**, 2689 (2000); S. Cheng, S. Petriconi, S. Pratt, M. Skoby, C. Gale, S. Jeon, V. T. Pop, and Q. H. Zhang, Phys. Rev. C **69**, 54906 (2004); P. Christakoglou, A. Petridis, and M. Vassiliou, Nucl. Phys. **A749**, 279c (2005).

[14] J. Adams *et al.* (STAR Collaboration), Phys. Rev. C **73**, 064907 (2006); Phys. Lett. **B634**, 347 (2006).

[15] J. Adams *et al.* (STAR Collaboration), Phys. Rev. C **68**, 044905 (2003).

[16] C. Adler *et al.* (STAR Collaboration), Phys. Rev. Lett. **90**, 082302 (2003).

[17] C. Adler *et al.* (STAR Collaboration), Phys. Rev. Lett. **87**, 112303 (2001); J. Adams *et al.* (STAR Collaboration), *ibid.* **92**, 112301 (2004).

[18] X. N. Wang and M. Gyulassy, Phys. Rev. D **44**, 3501 (1991).

[19] S. J. Lindenbaum and R. S. Longacre, Eur. Phys. J. C. **49**, 767 (2007).

[20] S. Eidelman *et al.*, Phys. Lett. **B592**, 1 (2004), see p. 279.